Materials Science & Engineering A 563 (2013) 125–132

Contents lists available at SciVerse ScienceDirect

Materials Science & Engineering A

journal homepage: www.elsevier.com/locate/msea

Tensile and fatigue properties of weld-bonded and adhesive-bonded magnesium alloy joints

W. Xu [a], L. Liu [b,d], Y. Zhou [b], H. Mori [c], D.L. Chen [a,*]

[a] Department of Mechanical and Industrial Engineering, Ryerson University, 350 Victoria Street, Toronto, Ontario M5B 2K3, Canada
[b] Department of Mechanical and Mechatronics Engineering, University of Waterloo, 200 University Avenue West, Waterloo, Ontario N2L 3G1, Canada
[c] Department of Management of Industry and Technology, Osaka University, 2-1 Yamadaoka, Suita, Osaka 565-0871, Japan
[d] Department of Mechanical Engineering, Tinghua University, Beijing 100084, China

ARTICLE INFO

Article history:
Received 16 September 2012
Received in revised form
2 November 2012
Accepted 15 November 2012
Available online 23 November 2012

Keywords:
Weld-bonding
Adhesive-bonding
Magnesium alloy
Tensile lap shear
Fatigue

ABSTRACT

The microstructures, tensile and fatigue properties of weld-bonded (WB) AZ31B-H24 Mg/Mg joints with different sizes of bonding area were evaluated and compared with the adhesive-bonded (AB) Mg/Mg joints. Typical equiaxed dendritic structures containing divorced eutectic $Mg_{17}Al_{12}$ particles formed in the fusion zone of both WB-1 (with a bonding area of 35 mm × 35 mm) and WB-0.5 (with a bonding area of 17.5 mm × 35 mm) joints. Less solidification shrinkage cracking was observed in the WB-0.5 joints than WB-1 joints. While the WB-0.5 joints exhibited a slightly lower maximum tensile shear stress than the AB-0.5 joints (with a bonding area of 17.5 mm × 35 mm), the energy absorption was equivalent. Although the AB-0.5 joints exhibited a higher fatigue resistance at higher cyclic stress levels, both the AB-0.5 and WB-0.5 joints showed an equivalent fatigue resistance at lower cyclic stress levels. A higher fatigue limit was observed in the WB-0.5 joints than in the WB-1 joints owing to the presence of fewer shrinkage pores. Cohesive failure mode along the adhesive layer in conjunction with partial nugget pull-out from the weld was observed at the higher cyclic loads, and fatigue failure occurred in the base metal at the lower cyclic loads.

1. Introduction

Due to the huge consumption on natural resources and global warming, many government legislations require the reduction in fuel consumption and anthropogenic greenhouse-gas emissions to protect our precious environment [1–6]. Manufacturers in the automotive and aerospace industries are counting on reducing vehicle weight via applying advanced lightweight materials to improve fuel efficiency and reduce CO_2 emissions [7–10]. Recently the development and application of ultra-lightweight magnesium alloys are significantly increasing in the transportation sectors due to their low density, high strength-to-weight ratio, and superior damping capacity [11–16]. The structural application of lightweight magnesium alloys inevitably involve welding and joining while guaranteeing the safety and reliability of motor vehicles.

Weld-bonding, a hybrid joining process developed originally to prevent noise and vibrations for aircraft, automobile production and railway carriages, combines resistance spot welding with adhesive-bonding. It could be used to reduce manufacturing costs, improve mechanical properties and corrosion resistance [17–22]. It has been reported that the bonding geometry is one of the key factors for the performance of weld-bonded (WB) joints and adhesive-bonded (AB) joints [23–27]. Goglio and Rossetto [23] studied an influence of geometry in the strength of AB steel joints and reported that the stress intensity factor decreases monotonically with increasing bonding area. Da Silva et al. [24] studied the effect of geometry on the shear strength of AB DIN St33 steel (a German DIN standard steel) to DIN C65 steel (a German DIN standard steel) joints and observed the lap shear strength (i.e., in the form of failure load) of the joint increased almost linearly with overlap. Fessel et al. [25] evaluated different AB joint geometries for automotive applications using FEA and concluded that the stress distribution largely depended on the geometry of a joint. Pirondi and Moroni [26] investigated fatigue behavior of AB 6082-T4 aluminum and S255 steel joints and noticed that at the same level of average shear stress, the shorter the joint, the longer the duration.

While a lot of studies have been reported on the WB/AB joints of steels and aluminum alloys, the research on WB or AB joints of magnesium alloys is limited. In our earlier study [27], the microstructures, tensile and fatigue properties of WB Mg/Mg joints and Mg/steel joints were evaluated and compared with resistance spot welded (RSW) Mg/steel joints. The results showed

* Corresponding author. Tel.: +1 416 979 5000x6487; fax: +1 416 979 5265.
E-mail address: dchen@ryerson.ca (D.L. Chen).

0921-5093/$ - see front matter © 2012 Elsevier B.V. All rights reserved.
http://dx.doi.org/10.1016/j.msea.2012.11.049

that both WB Mg/Mg and Mg/steel joints were significantly stronger than RSW Mg/steel joints in both fatigue and tensile tests. However, it is still unclear how the geometry or the size of bonding area influences the microstructure and mechanical properties of WB Mg/Mg joint. The objective of the present study was, therefore, to identify the influence of bonding geometry or overlap area on the microstructures, tensile properties and fatigue strength of WB Mg/Mg joints.

2. Material and experimental procedure

2.0 mm thick AZ31B-H24 Mg sheet alloy with a composition (wt%) of 2.92 Al, 1.09 Zn, 0.3 Mn, and 0.01 Si was selected in the present study. The test coupons of 35 mm in width and 100 mm in length were cut for WB and AB Mg/Mg joint. Prior to bonding, specimens were ultrasonically cleaned for 5 min followed by chemical cleaning using a solution of 2.5% (weight/volume) chromic acid to remove surface oxides. For the AB specimens, Terokal® 5087-02P adhesive was applied and then cured at a temperature of 180 °C for 30 min (Fig. 1(a and b)). For the WB specimens, resistance spot welding (Fig. 1(c)) was performed, followed by the curing (Fig. 1(d)). The resistance spot welding parameters were selected to be 8 kA, three cycles plus 24 kA, eight cycles using alternate current (AC). An electrode cap (type FF25) with a sphere radius of 50.8 mm and a face diameter of 16 mm was used for WB Mg/Mg similar welding. Two types of WB joints were made in this study: WB-1 (weld-bonded joints with a bonding overlap of 35 mm × 35 mm) as shown in Fig. 2(a), and WB-0.5 (weld-bonded joints with a bonding overlap of 17.5 mm × 35 mm) as seen in Fig. 2(b). Fig. 2(c) shows the geometry of the AB-0.5 adhesive bonded joints with a bonding area of 17.5 mm × 35 mm.

The metallographic samples were sectioned across the weld center parallel to the loading direction, and then cold mounted, ground, polished and etched with a solution of 4.2 g picric acid, 10 ml acetic acid, 70 ml ethanol, and 10 ml water. An optical microscope in conjunction with Clemex quantitative image analysis system was used to observe the microstructures of weld nuggets and base metal (BM). Tensile tests were carried out at room temperature using a fully computerized United tensile testing machine at different crosshead speeds of 0.1 mm/min, 1.0 mm/min and 10.0 mm/min for each group. The displacement during the tensile shear tests was recorded by computer according to the relative change of the upper and lower grips. Two samples were tested at each crosshead speed. Fatigue tests were performed using a fully computerized Instron 8801 servo-hydraulic testing system under load control at different maximum loads. A load ratio of R (P_{min}/P_{max}) equal to 0.2, sinusoidal waveform, and frequency of 50 Hz were used in all the tests. Two samples were tested at each cyclic load level. To prevent the rotation and bending moment of the specimen during the tensile and fatigue tests, two spacers with a thickness of 2 mm, a width of 35 mm and a length of 35 mm were attached at both ends of the specimen (Fig. 2(d)). The fracture surface morphology and microstructures were examined using a JSM-6380LV scanning electron microscope (SEM) equipped with Oxford energy dispersive X-ray spectroscopy (EDS) system and 3D fractographic analysis capacity.

3. Results and discussion

3.1. Microstructure

The overall weld nugget and microstructure of WB-1 Mg/Mg joint are shown in Fig. 3. The cross-section of the weld (Fig. 3(a)) experienced a microstructural change as reported in our earlier

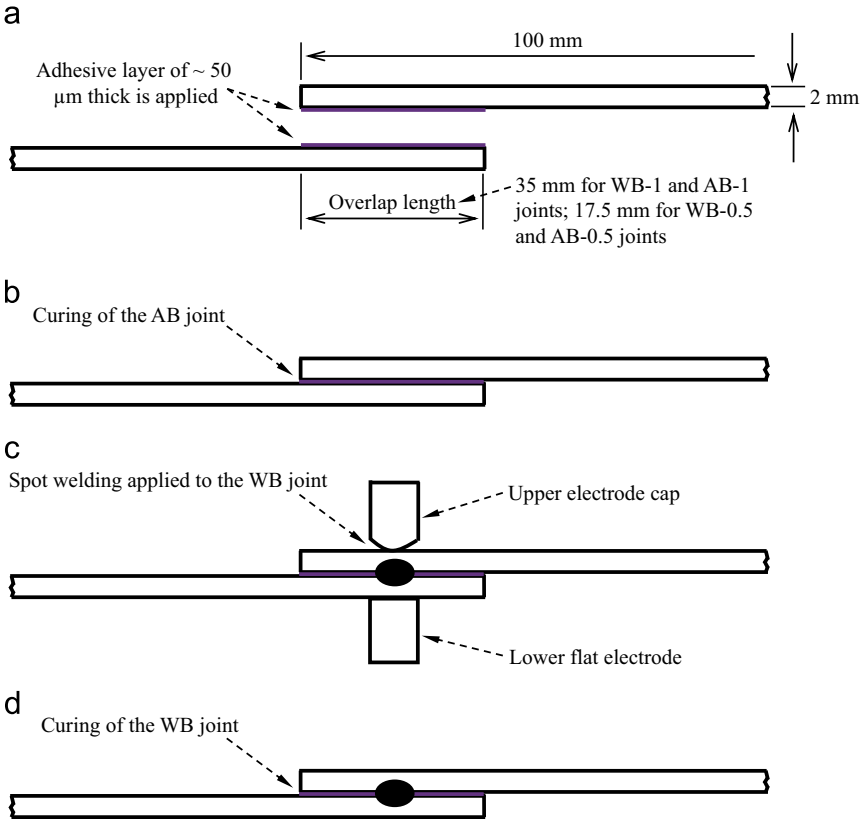

Fig. 1. Schematic diagram of the AB and WB Mg/Mg joints showing (a) adhesive layers applied to both top and bottom sheets, (b) curing of the AB joint specimen at a temperature of 180 °C for 30 min, (c) spot welding conducted before curing, and (d) curing of the WB joint specimen at a temperature of 180 °C for 30 min.

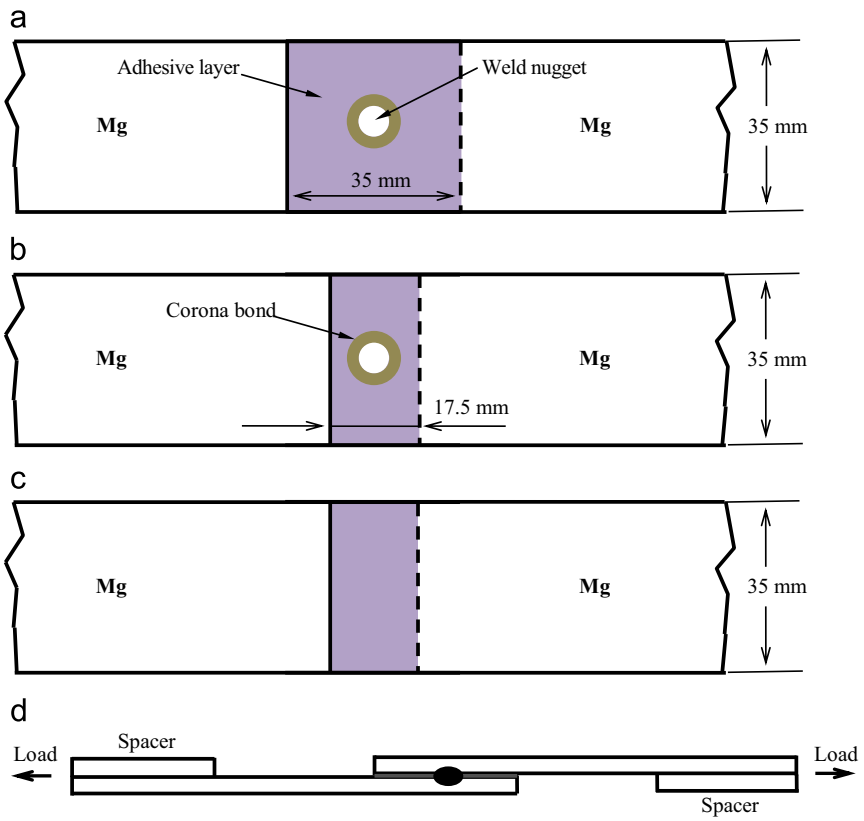

Fig. 2. Schematic illustration of (a) WB-1 Mg/Mg joint, (b) WB-0.5 Mg/Mg joint, (c) AB-0.5 Mg/Mg joint, and (d) tensile and fatigue test specimens with two spacers.

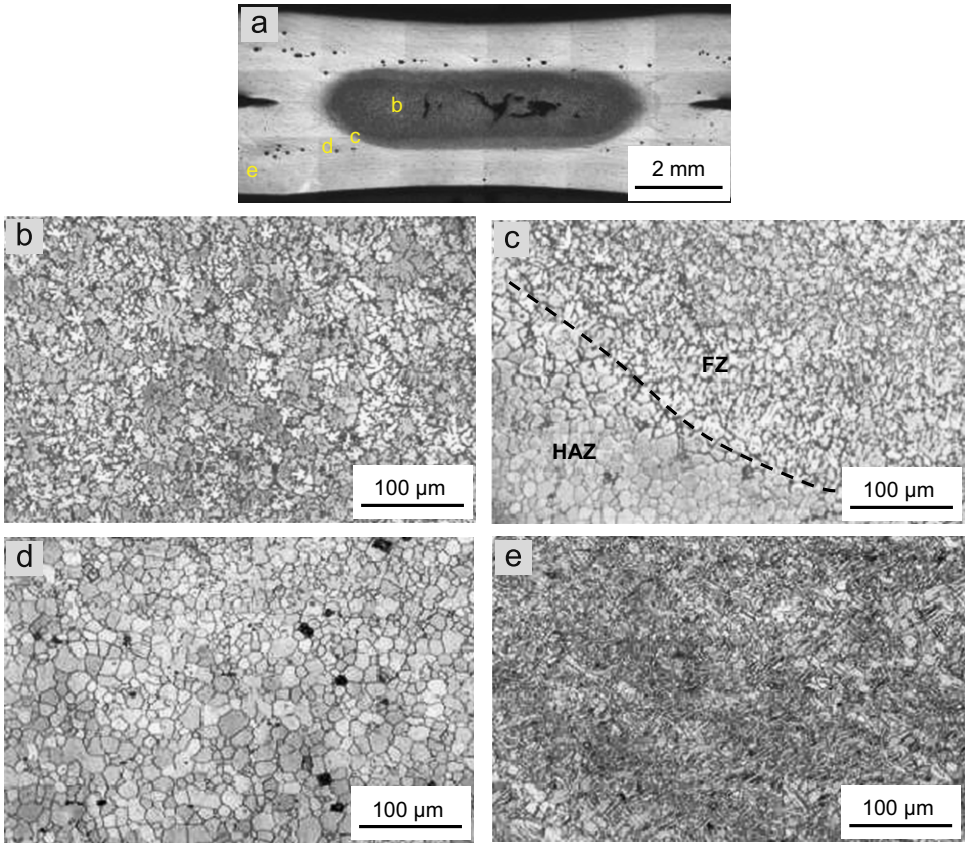

Fig. 3. Microstructures of a WB-1 Mg/Mg joint, (a) overall view of nugget where the location of the subsequent images is indicated, (b) equiaxed dendritic structure within fusion zone (FZ), (c) microstructure near the FZ border, (d) heat-affected zone (HAZ) and (e) base metal (BM).

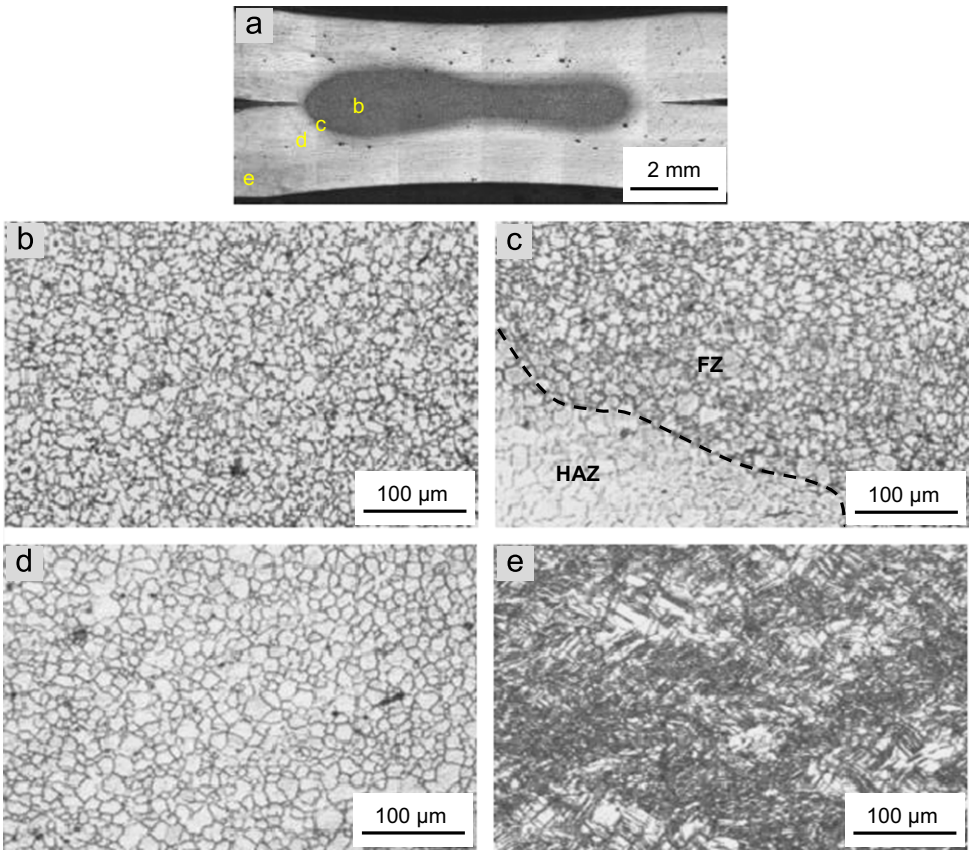

Fig. 4. Microstructures of a WB-0.5 Mg/Mg joint, (a) overall view of nugget where the position of the subsequent images is indicated, (b) equiaxed dendritic structure with FZ, (c) microstructure near the FZ border, (d) HAZ, and (e) BM.

study [27]. The microstructure of the weld nugget consisted of equiaxed dendrites containing divorced eutectic $Mg_{17}Al_{12}$ particles [28–33], which were mainly located at the interdendritic and intergranular regions (Fig. 3(b)). Little divorced eutectic $Mg_{17}Al_{12}$ particles in the heat-affected zone (HAZ) were observed, as shown in Fig. 3(c and d), where HAZ was characterized by equiaxed recrystallized grains. Fig. 3(e) shows the microstructure in the BM AZ31B-H24 Mg alloy which consisted of deformed and elongated grains, similar to those reported in [34–42].

The weld nugget and microstructural changes across a WB-0.5 joint are shown in Fig. 4. The microstructure in the nugget of the WB-0.5 joint also consisted of equiaxed dendrites and $Mg_{17}Al_{12}$ particles located at the interdendritic and intergranular regions as seen from Fig. 4(a); no or little divorced eutectic $Mg_{17}Al_{12}$ particles in the HAZ of the WB-0.5 joint were present, as shown in Fig. 4(b and c). By comparing the WB-1 with WB-0.5 joints, less solidification cracking or shrinkage was observed in the WB-0.5 joints. This might be due to a slower cooling rate in the cooling phase after RSW when reducing the bonding overlap area. It is known that most of the heat was diffused by cooling water in the electrodes during RSW. Other means of heat loss/transfer would be through Mg alloy itself and the surrounding air. Since the thermal conductivity of Mg (about 10^2 to 10^3 W/m K) was much higher than that of air (about 10^{-4} to 10^{-6} W/m K) [43], the heat transfer by Mg workpieces would be more important in a weld bonding process. A smaller overlap area of the WB-0.5 joint (Fig. 2(b)), relative to the WB-1 joint (Fig. 2(a)), represented a smaller or less efficient heat transfer area and a lower heat storage volume or capacity. This would result in a lower cooling rate in the WB-0.5 joint, which was helpful for reducing pores and hot cracks [44,45]. On the other hand, when the overlap bonding area was larger, it was hard to squeeze the adhesive out of the fusion zone because of the poor liquidity of the adhesive. Once adhesives were trapped in the nugget during resistant spot welding processing, pores could be induced since the adhesives were made by epoxy and could be gasified when heating up. Therefore, WB-0.5 joints exhibited fewer pores in the nugget than WB-1 joints, as shown in Fig. 4(a) vs. Fig. 3(a).

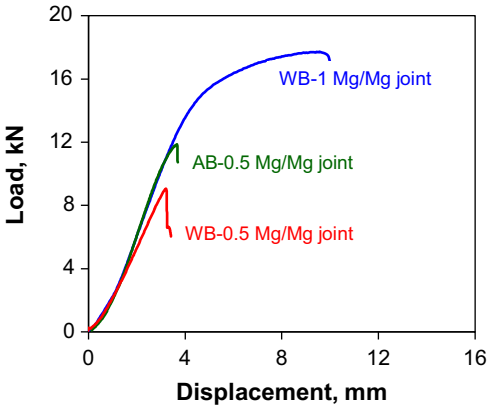

Fig. 5. Tensile shear load vs. displacement for the WB-1 Mg/Mg joint, WB-0.5 Mg/Mg joint and AB-0.5 Mg/Mg joint tested at a crosshead speed of 0.1 mm/min.

3.2. Tensile properties

Typical curves of the applied tensile shear load versus displacement for WB-1, WB-0.5 and AB-0.5 joints are shown in Fig. 5. The WB-1 joint was stronger than both WB-0.5 and AB-0.5 joints because of the twice larger bonding area, while the maximum

load of the WB-0.5 joint was slightly lower than that of the AB-0.5 joint. This might be due to the fact that the spot weld of WB joints would have some less favorable effect on the stress distribution during tensile lap shear tests as reported by Chang et al. [17,46] based on their both experimental and numerical results on a 08Al steel sheet (a car body steel sheet) and SHA-2858 II epoxy-based adhesives, where the welding heat and welding force destroyed/squeezed the adhesive layer and resulted in a reduction in the actual loading area and an increase in both normal stress (within the weld nugget) and shear stress (near the border of the nugget) [46]. Similar stress distributions in the weld nugget across a WB joint via a finite element analysis were reported in [47].

The evaluated maximum tensile shear stress (i.e., the maximum tensile load divided by the overlap area) is shown in Fig. 6(a). It is seen that the maximum tensile shear stress of WB-1, WB-0.5 and AB-0.5 joints increased with increasing crosshead speed. The WB-0.5 joints had a higher maximum tensile shear stress than the WB-1 joints, while it was slightly lower than that of AB-0.5 joints. A similar result was reported by Liu and Ren [48] by comparing a metal inert gas (MIG) spot weld bonding with an adhesive bonding on AZ31 Mg alloy and 6061 Al alloy sheets, where the tensile shear test showed that the strength of MIG spot weld bonding (maximum tensile shear load: 5.3 kN) was slightly lower than that of the adhesive bonding (maximum tensile shear load: 6.0 kN), and both were much higher than that of the MIG spot welding (maximum tensile shear load: 1.7 kN). The energy absorption (i.e., the area below a load–displacement curve in Fig. 5) was estimated as well. As seen from Fig. 6(b), with increasing crosshead speed the energy absorption of the WB-1 joints obviously increased, while the absorbed energy of WB-0.5 and AB-0.5 joints kept nearly constant and was equivalent.

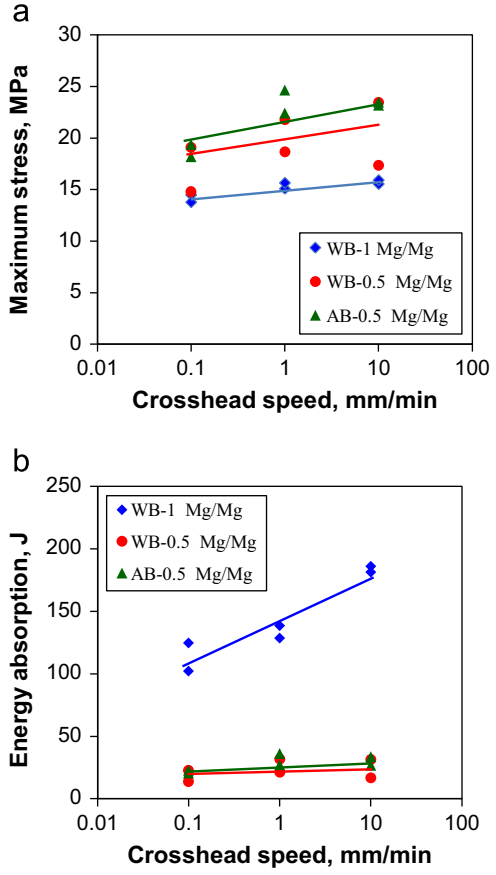

Fig. 6. (a) Maximum tensile shear stress and (b) the energy absorption versus the crosshead speed for the WB-1 Mg/Mg, WB-0.5 Mg/Mg and AB-0.5 Mg/Mg joints.

3.3. Fatigue strength and failure mode

Fig. 7 presented the maximum tensile shear cyclic stress versus the number of cycles to failure of WB-1, WB-0.5 and AB-0.5 joints, obtained at RT, $R=0.2$, and a frequency of 50 Hz. It is seen that at higher stress levels the AB-0.5 joints showed the highest fatigue resistance because of a uniform stress distribution. The fatigue life of the WB-0.5 joints was shorter than that of the AB-0.5 joints at the same maximum stress level. Similar results on the fatigue life of 08Al steel joints with SHA-2858 II epoxy-based adhesives were reported by Chang et al. [46], where the adhesive-bonded joints had a longer fatigue life than the weld-bonded joints at all cyclic loading levels applied. As discussed above, the presence of the un-bonded area (i.e., the plastic ring or corona bond at the peripheral area of the nugget shown in Fig. 2(a) and (b)) induced by the electrode force could increase the local stress at both the notch of the weld nugget and the edge of the adhered overlap [46,47]. The higher stress made the fatigue crack initiation and growth from the weld cavities easier [46,49,50]. Both WB-1 and WB-0.5 joints performed equivalently with respect of fatigue life at the low cycle fatigue regime (e.g., at a higher cyclic stress level of ~12 MPa). However, at the high cycle fatigue regime (or lower cyclic stress levels), WB-0.5 joints showed a longer fatigue life than WB-1 joints because of the fewer solidification or shrinkage cracks in the nugget in WB-0.5 joints as shown in Fig. 4(a). This corresponded well to that presented by Roesler et al. [51] who pointed out that the fatigue strength of a material under dynamic cyclic loading was much more susceptible to the manufacturing process and materials than the static strength. The fatigue strength was also much more sensitive to the lower level cyclic load than the higher level cyclic load.

Fig. 8 presents the failure mode in conjunction with the logarithmic S–N plots in the form of the maximum tensile shear cyclic stress versus the number of reversals to failure ($2N_f$) in terms of Basquin type relationship. It should be noted that the run-out data for the non-failed samples at or over 1×10^7 cycles were not included in the fitting. For all the WB-1, WB-0.5 and AB-0.5 joints tested, cohesive failure mode along the adhesive layer was observed at the higher cyclic load levels, and BM failure occurred at the lower cyclic load levels (Fig. 8). It is worthwhile to mention that the cohesive failure (i.e., failure occurs within the adhesive layer) is different from the adhesive failure (i.e., failure occurs in-between the adhesive layer and adherent interfacially) and the adherent failure (i.e., failure occurs within the adherent). The cohesive failure is most desirable as it assures the use of the maximum strain energy by the weaker part of the joint, which is usually the adhesive [52–54]. It is seen from the inserts in Fig. 8(a–c) that the adhesive failure occurred at the high cyclic stress levels for all the three types of joints tested in the present

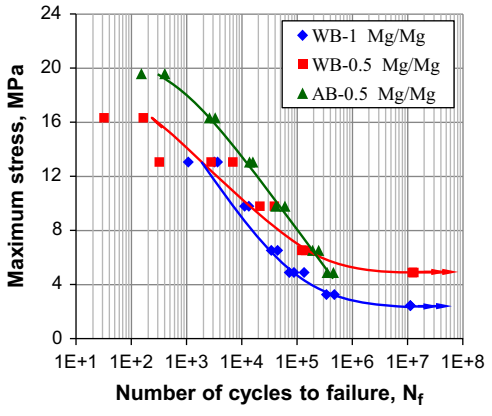

Fig. 7. S–N curves of the WB-1 Mg/Mg, WB-0.5 Mg/Mg and AB-0.5 Mg/Mg joints tested at RT, $R=0.2$, and a frequency of 50 Hz.

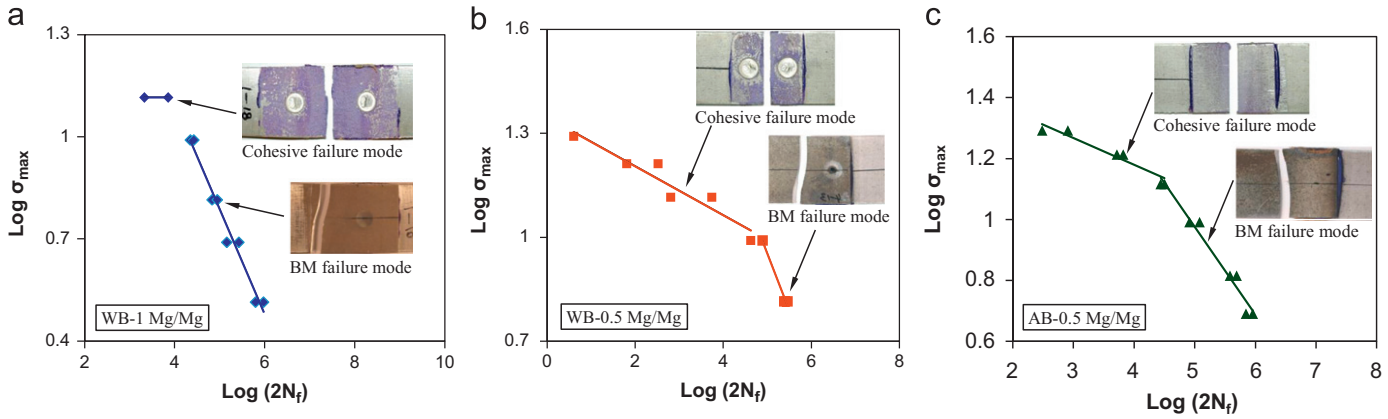

Fig. 8. Maximum tensile shear cyclic stress vs. the number of reversals to failure ($2N_f$) in the double-log scale for (a) WB-1 Mg/Mg joints, (b) WB-0.5 Mg/Mg joints, and (c) AB-0.5 Mg/Mg joints.

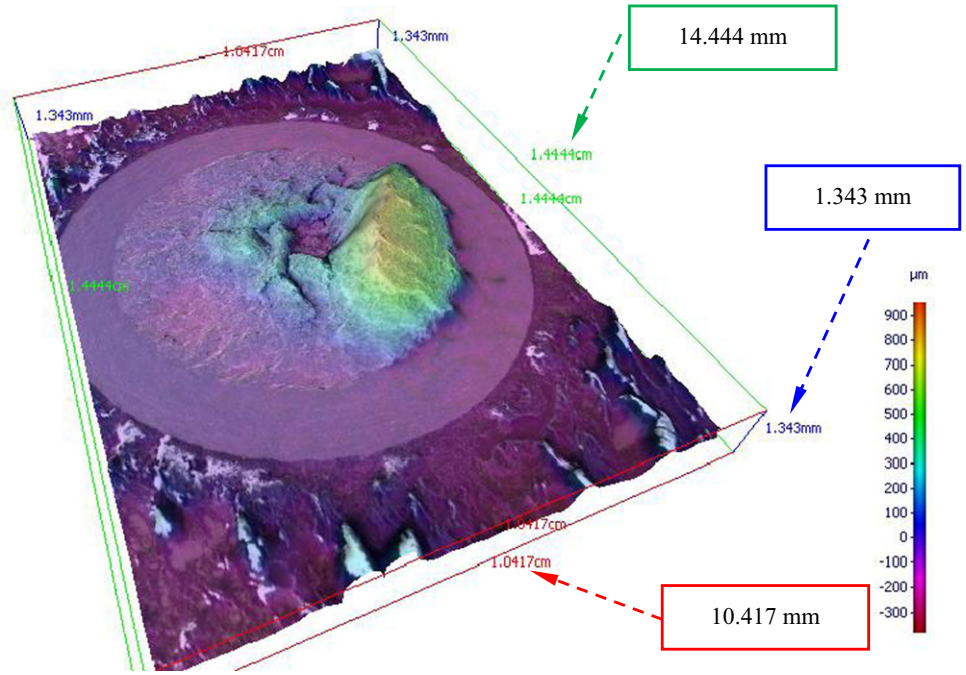

Fig. 9. A typical 3D SEM image showing the partial button pull-out of a WB-0.5 Mg/Mg joint after fatigue test at an applied maximum cyclic load of 16 kN (Dimensions of the "observation box": 14.444 mm × 10.417 mm × 1.343 mm).

study, since the applied adhesive remained stuck to both sides of the overlap portion. When the cohesive failure occurred in the above samples, partial nugget pull-out from the weld was also observed in the WB-0.5 and WB-1 joints, as shown in Fig. 9(a) maximum cyclic load of 16 kN for a WB-0.5 joint.

The change of the failure mode from the cohesive failure to the BM failure occurred at Log σ_{max}=1.12 or σ_{max}=13.1 MPa in the WB-1 joints (Fig. 8(a)). It was observed that both samples fatigued at the maximum cyclic stress of 13.1 MPa failed in the mode of cohesive failure, while all other samples tested below the above maximum cyclic stress failed in the BM. Due to the half overlap area in the WB-0.5 joints (Fig. 2(b)), the change of the failure mode from the cohesive failure to the BM failure occurred at Log σ_{max}=0.99 or σ_{max}=9.8 MPa (Fig. 8(b)). At this cyclic stress level one sample failed in the BM and the other failed by the cohesive mode, above which all the tested samples failed in the cohesive mode, and below which all the samples failed in the BM. Likewise, such a transition of failure mode from the upper cohesive failure to the lower BM failure occurred at Log σ_{max}=1.12 or σ_{max}=13.1 MPa in the AB-0.5 joints as well (Fig. 8(c)).

3.4. Fractography

To observe more details on the fracture surface, SEM images of the failed WB-1 and WB-0.5 joints are shown in Figs. 10 and 11 which were tested at a maximum cyclic load of 16 kN (or σ_{max}=13.1 MPa) and 10 kN (or σ_{max}=16.3 MPa), respectively. It can be seen from Fig. 10(a) that fatigue crack could be developed from the point "d" and propagated along the faying surface and through the nugget. The typical elliptical shear deformation characteristics as shown in Fig. 10(b) and (c) reflected that shear stress dominated both fatigue crack initiation and propagation, and final rapid failure. Free solidified dendritic structure was observed in the center of the nugget, as shown in Fig. 10(d) at a higher magnification. The shrinkage pores in the nugget of the WB-1 joint (Fig. 10(a)) were more than that of the WB-0.5 joint

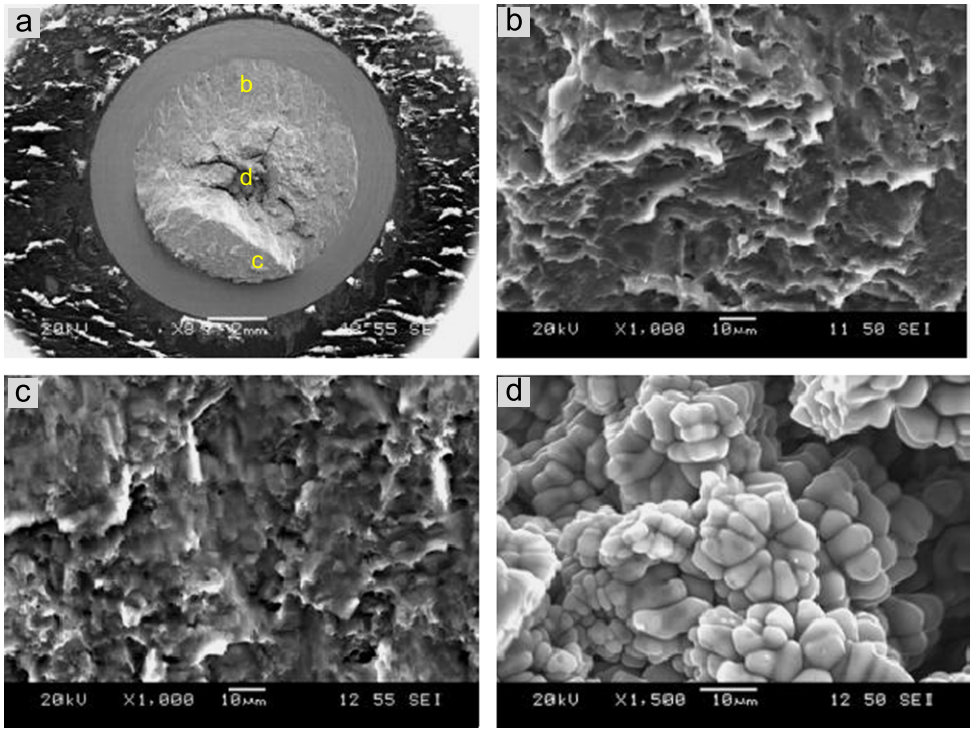

Fig. 10. SEM images of fatigue fracture surface of a WB-1 Mg/Mg joint tested at an applied maximum cyclic load of 16 kN, (a) overall view, (b) facet-like shear deformation features near the interfacial surface, (c) facet-like shear deformation features at the top of partial pull-out button, and (d) shrinkage pore in the weld nugget.

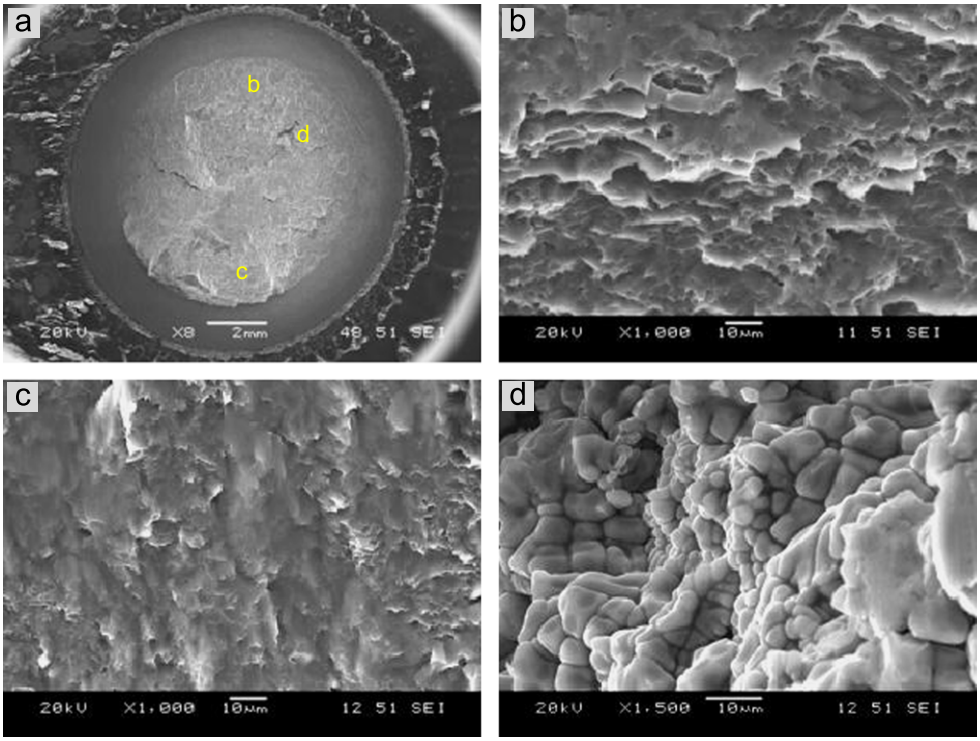

Fig. 11. SEM images of fatigue fracture surface of a WB-0.5 Mg/Mg joint tested at an applied maximum cyclic load of 10 kN, (a) overall view, (b) facet-like shear deformation features near the interfacial surface, (c) facet-like shear deformation features at the top of partial pull-out button, and (d) shrinkage pore in the weld nugget.

(Fig. 11(a)), which matched well with the cross-section observations shown in Fig. 3(a) and (a). This would be the reason why a higher fatigue resistance or a longer fatigue life at a given maximum cyclic stress was observed in the WB-0.5 joints, as shown in Fig. 7(a). Except the above difference, the fracture surface of the WB-0.5 joint displayed basically a similar feature

to that of the WB-1 joint, such as the typical elliptical shear deformation characteristics (Fig. 11(b) and (c)) and free solidified dendritic structure (Fig. 11(d)).

4. Conclusions

(1) In both WB-1 Mg/Mg joints with a lager bonding area of 35 mm × 35 mm and WB-0.5 Mg/Mg joints with a smaller (half) bonding area of 17.5 mm × 35 mm, typical equiaxed dendritic structures containing divorced eutectic $Mg_{17}Al_{12}$ particles formed in the FZ, while less severe solidification shrinkage pores were observed to be present in the WB-0.5 joints. The HAZ in both types of joints was characterized by equiaxed recrystallized grains.

(2) Although the WB-0.5 joints exhibited a slightly lower maximum tensile shear stress than the adhesive-bonded AB-0.5 joints with a bonding area of 17.5 mm × 35 mm due to the reduction of actual loading area and the increase in the stress across the weld nugget in the WB-0.5 joints, the energy absorption was equivalent. However, the energy absorption of WB-1 joints was much higher due to the larger bonding area, which also increased with increasing crosshead speed.

(3) The AB-0.5 joints exhibited a higher fatigue resistance at higher cyclic stress levels because of the presence of a uniform stress distribution in the bonding area, while the WB-0.5 joints showed an equivalent fatigue resistance at lower cyclic stress levels. Also, a higher fatigue limit was observed for the WB-0.5 joints compared with the WB-1 joints due to the presence of fewer solidification shrinkage pores.

(4) In all the joints tested, cohesive failure mode along the adhesive layer was observed at the higher cyclic stress levels, and fatigue failure occurred in the base metal at the lower cyclic stress levels. The cohesive failure in the weld-bonded joints was often accompanied by the occurrence of partial nugget pull-out from the weld.

Acknowledgments

The authors would like to thank the Natural Sciences and Engineering Research Council of Canada (NSERC), Automotive Partnership Canada (APC), and AUTO21 Network of Centers of Excellence for providing financial support. This investigation involves part of Canada–China–USA Collaborative Research Project on the Magnesium Front End Research and Development (MFERD). The authors also thank General Motors Research and Development Center for the supply of test materials. One of the authors (D.L. Chen) is grateful for the financial support by the Premier's Research Excellence Award (PREA), NSERC-Discovery Accelerator Supplement (DAS) Award, Canada Foundation for Innovation (CFI), and Ryerson Research Chair (RRC) program. The assistance of Q. Li, A. Machin, J. Amankrah, and R. Churaman in performing the experiments is gratefully acknowledged. The authors also thank Dr. X. Cao, Dr. S. Xu, Dr. K. Sadayappan, Dr. M.S. Kozdras, Dr. J. Jackman, Professor N. Atalla, Professor S. Lambert, Professor H. Jahed, Professor Y.S. Yang, Professor M.F. Horstemeyer, Professor B. Jordon, Professor J. Allison, Dr. A.A. Luo, Dr. A. Khosrovaneh, Mr. R. Osborne, Mr. J.F. Quinn, Dr. X.M. Su, and Mr. L. Zhang for the helpful discussion.

References

[1] M. Wise, K. Calvin, A. Thomson, L. Clarke, B. Bond-Lamberty, R. Sands, S.J. Smith, A. Janetos, J. Edmonds, Science 324 (2009) 1183–1186.
[2] D. Shindell, G. Faluvegi, M. Walsh, S.C. Anenberg, R.V. Dingenen, N.Z. Muller, J. Austin, D. Koch, G. Milly, Nat. Clim. Change 1 (2011) 59–66.
[3] Q. Schiermeier, Nature 470 (2011) 316.
[4] P. Pall, T. Aina, D.A. Stone, P.A. Stott, T. Nozawa, A.G.J. Hilberts, D. Lohmann, M.R. Allen, Nature 470 (2011) 382–385.
[5] H.J. Kim, C. McMillan, G.A. Keoleian, S.J. Skerlos, J. Ind. Ecol. 14 (2010) 929–946.
[6] L.R. Kump, Nature 419 (2002) 188–190.
[7] H. Kang, I. Accorsi, B. Patel, E. Pakalnins, Procedia Eng. 2 (2010) 129–138.
[8] H.Y. Wang, L.M. Liu, Z.Y. Jia, J. Mater. Sci. 46 (2011) 5534–5540.
[9] R. Braun, Mater. Sci. Eng. A 426 (2006) 250–262.
[10] H. Friedrich, S. Schumann, J. Mater. Process. Technol. 117 (2001) 276–281.
[11] B.L. Mordike, T. Ebert, Mater. Sci. Eng. A 302 (2001) 37–45.
[12] T.M. Pollock, Science 328 (2010) 986–987.
[13] S.J. Liang, H.F. Sun, Z.Y. Liu, E. Wang, J. Alloys Compd. 472 (2009) 127–132.
[14] G.B. Hamu, D. Eliezer, L. Wagner, J. Alloys Compd. 468 (2009) 222–229.
[15] Y.R. Wang, Z.H. Mo, J.C. Feng, Z.D. Zhang, Sci. Technol. Weld. Joining 12 (2007) 641–646.
[16] J.B. Jiang, Z.D. Zhang, J. Alloys Compd. 466 (2008) 368–372.
[17] B.H. Chang, Y.W. Shi, S.J. Dong, J. Mater. Process. Technol. 100 (2000) 171–178.
[18] V.M. Goncalves, P.A.F. Martins, Mater. Manuf. Process. 21 (2006) 774–778.
[19] I.O. Santos, W. Zhang, V.M. Goncalves, N. Bay, P.A.F. Martins, Int. J. Mach. Tools Manuf. 44 (2004) 1431–1439.
[20] A. Higgins, Int. J. Adhes. Adhes. 20 (2000) 367–376.
[21] L.M. Liu, J.B. Jiang, IEEE Trans. Plasma Sci. 39 (2011) 581–586.
[22] S.M.H. Darwish, A. Ghanya, J. Mater. Process. Techol. 105 (2000) 221–229.
[23] L. Goglio, M. Rossetto, Int. J. Adhes. Adhes. 30 (2010) 313–321.
[24] L.F.M. da Silva, R.J.C. Carbas, G.W. Critchlow, M.A.V. Figueiredo, K. Brown, Int. J. Adhes. Adhes. 29 (2009) 621–632.
[25] G. Fessel, J.G. Broughton, N.A. Fellows, J.F. Durodola, A.R. Hutchinson, Int. J. Adhes. Adhes. 27 (2007) 574–583.
[26] A. Pirondi, F. Moroni, Int. J. Adhes. Adhes. 29 (2009) 796–805.
[27] W. Xu, D.L. Chen, L. Liu, H. Mori, Y. Zhou, Mater. Sci. Eng. A 537 (2012) 11–24.
[28] S. Barbagallo, H.I. Laukli, O. Lohne, E. Cerri, J. Alloys Compd. 378 (2004) 226–232.
[29] I.P. Moreno, T.K. Nandy, J.W. Jones, J.E. Allison, T.M. Pollock, Scr. Mater. 45 (2001) 1423–1429.
[30] J. Cai, G.C. Ma, Z. Liu, H.F. Zhang, Z.Q. Hua, J. Alloys Compd. 422 (2006) 92–96.
[31] H.A. Patel, N. Rashidi, D.L. Chen, S.D. Bhole, A.A. Luo, Mater. Sci. Eng. A 546 (2012) 72–81.
[32] H.A. Patel, D.L. Chen, S.D. Bhole, K. Sadayappan, J. Alloys Compd. 496 (2010) 140–148.
[33] H.A. Patel, D.L. Chen, S.D. Bhole, K. Sadayappan, Mater. Sci. Eng. A 528 (2010) 208–219.
[34] S.M. Chowdhury, D.L. Chen, S.D. Bhole, X. Cao, E. Powidajko, D.C. Weckman, Y. Zhou, Mater. Sci. Eng. A 527 (2010) 2951–2961.
[35] S.M. Chowdhury, D.L. Chen, S.D. Bhole, E. Powidajko, D.C. Weckman, Y. Zhou, Metall. Mater. Trans. A 42 (2011) 1974–1989.
[36] S.M. Chowdhury, D.L. Chen, S.D. Bhole, X. Cao, Mater. Sci. Eng. A 527 (2010) 6064–6075.
[37] S.H. Chowdhury, D.L. Chen, S.D. Bhole, E. Powidajko, D.C. Weckman, Y. Zhou, Metall. Mater. Trans. A 43 (2012) 2133–2147.
[38] S.H. Chowdhury, D.L. Chen, S.D. Bhole, X. Cao, P. Wanjara, Mater. Sci. Eng. A 556 (2012) 500–509.
[39] S.H. Chowdhury, D.L. Chen, S.D. Bhole, X. Cao, P. Wanjara, Metall. Mater. Trans. A (2012) 9 (accepted in July 2012).
[40] N. Afrin, D.L. Chen, X. Cao, M. Jahazi, Mater. Sci. Eng. A 472 (1–2) (2008) 179–186.
[41] N. Afrin, D.L. Chen, X. Cao, M. Jahazi, Scr. Mater. 57 (2007) 1004–1007.
[42] M. Fairman, N. Afrin, D.L. Chen, X.J. Cao, M. Jahazi, Can. Metall. Q. 46 (2007) 425–432.
[43] L.M. Liu, J.B. Jiang, J. Mater. Process. Technol. 209 (2009) 2864–2870.
[44] B. Lang, D.Q. Sun, Z.Z. Xuan, X.F. Qin, ISIJ Int. 48 (2008) 77–82.
[45] Y.R. Wang, Z.D. Zhang, Trans. China Weld. Inst. 27 (2006) 9–12.
[46] B.H. Chang, Y.W. Shi, L.Q. Lu, J. Mater. Process. Technol. 108 (2001) 307–313.
[47] A. Al-Samhan, S.M.H. Darwish, J. Mater. Process. Techol. 142 (2003) 587–598.
[48] L.M. Liu, D.X. Ren, Mater. Des. 32 (2011) 3730–3735.
[49] P.C. Wang, S.K. Chisholm, G. Banas, F.V. Lawrence, Weld. J. 2 (1995) 41–47.
[50] A. Al-Samhan, S.M.H. Darwish, Int. J. Adhes. Adhes. 23 (2003) 23–28.
[51] J. Roesler, H. Harders, M. Baeker, Mechanical Behavior of Engineering Materials: Metals, Ceramics, Polymers, and Composites, 1st Edition, Springer publication, Germany, 2007.
[52] N.M. Rahman, A. Mian, G.M. Newaz, ASME 2004 International Mechanical Engineering Congress and Exposition (IMECE2004), Paper no. IMECE2004-60939, pp. 129–135.
[53] M.E. Somervuori, M.T. Alenius, T. Kosonen, R. Karppi, H.E. Hanninen, Mater. Corros. 57 (2006) 562–567.
[54] M.D. Banea, L.F.M. da Silva, Materialwissenschaft und Werkstofftech, 41 (2010) 325–335.